Journal of Solid State Electrochemistry (2021) 25:2539–2548
https://doi.org/10.1007/s10008-021-05038-1

ORIGINAL PAPER

Effect of ex situ hydrogenation on the structure and electrochemical properties of amorphous silicon thin film

Hai-min Zhang[1,2,3] · Yong-chun Luo[1,2] · Song-ting Yang[2] · Yu-jie Xiang[2]

Received: 7 May 2021 / Revised: 20 August 2021 / Accepted: 23 August 2021 / Published online: 29 August 2021

Abstract

Nickel-metal hydride (Ni-MH) batteries were widely used due to their various advantages, but its further application and development have been seriously hindered by the low electrochemical discharge capacity of conventional hydrogen storage alloy electrode. The hydrogenated amorphous silicon (a-Si:H) thin film electrode for Ni-MH battery has been proven to have a dramatic electrochemical capacity. We prepared a-Si:H thin films by a two-step process of rf-sputtering followed by hydrogenation, and investigated the effect of hydrogenation on the structure and electrochemical properties of which as an anode. The maximum discharge capacity of a-Si:H thin film electrode after hydrogenation increases from initial 180 mAh·g^{-1}to 1827 mAh·g^{-1}, which is over tenfold that of as-deposited hydrogen-less a-Si thin film electrode. Then, the preliminary relationships between hydrogen content and electrochemical performance of a-Si:H thin film electrode were analyzed, and several negative factors of electrochemical performance for a-Si:H thin film electrode were proposed.

Keywords Hydrogenated amorphous silicon · Hydrogenation · Ionic liquid electrolyte · Electrochemical performance

Introduction

The benign and sustainable development of human society has been seriously affected and restricted by resource exhaustion and environmental deterioration that are caused by excessive use of traditional petrochemical energy [1, 2]. Nickel-metal hydride (Ni-MH) batteries have been widely used in new energy vehicles, portable electronic devices, emergency devices, and military equipment due to their advantages of good environmental compatibility, no pollution, safety and stability, fast dynamic response speed, and high-power efficiency [3–5]. However, the low electrochemical capacity of conventional hydrogen storage alloy electrode has seriously hindered the further application and development of Ni-MH battery [6–8].

Silicon (Si) materials have excellent performance in hydrogen storage as well as in the fields of microelectronic devices, photocatalysis, photovoltaic cells, lithium-ion battery, hydrogenation inorganic materials, and so on [9–11]. Theoretically, silicon hydrogen (SiH_x) has a maximum hydrogen content of 3.44, 6.66, and 9.67 wt% for x = 1, 2, and 3, respectively [12]. A variety of silicon nanostructures have also demonstrated to have impressive hydrogen storage performance. For instance, by using the first principle calculations, the gravimetric adsorption capacities of hydrogen in (9,9) silicon nanotube (SiNT) arrays reach up to 1.30, 2.33, and 2.88 wt% at the temperature of 298 K at the pressure of 2, 6, and 10 MPa, respectively [13]. The hydrogen of total gravimetric density of 9.48 wt% can be stored into the interior cavity of hydrogenated silicon fullerenes ($Si_{60}H_{60}$) [14]. The hydrogen of gravimetric percentage from 10.17 to 12.50 wt% are stored in the multifarious stable per-hydrogenated inorganic $Si_{20}H_{20}$ nanocage which was functionalized by replacing hydrogen atoms with small organic molecules of $-CN_2H_3$ (or $CONH_2$) and lithium atoms [15].

Although the theoretical electrochemical hydrogen storage capacity of silicon electrode is as high as 3826 mAh·g^{-1}, the porous silicon electrodes (PS) and amorphous silicon

✉ Hai-min Zhang
30083085@qq.com

✉ Yong-chun Luo
gdluoyc20180213@163.com

1 State Key Laboratory of Advanced Processing and Recycling of Nonferrous Metals, Lanzhou University of Technology, Lanzhou, China

2 School of Materials Science and Engineering, Lanzhou University of Technology, Lanzhou, China

3 School of Science, Lanzhou University of Technology, Lanzhou, China

(a-Si) electrodes have been experimentally confirmed to perform well in electrochemical hydrogen storage by only a few researchers. It is demonstrated that, in sulfuric acid (3 M H_2SO_4) electrolyte, the nano-porous silicon layer electrodes that are elaborated by electrochemical anodization of Si (100) with resistivity of 1 ~ 10 and 0.5 Ω•cm have electrochemical discharge capacity of about 86 and 232 mAh·g^{-1}, respectively [16, 17]. The highest hydrogen storage capacity of which can be greatly increased to 546.1 mAh·g^{-1} by coating with palladium and graphene oxide [17]. Hydrogenated amorphous silicon (a-Si:H) thin film electrodes deposited by plasma enhanced chemical vapor deposition (PECVD) were demonstrated to have a maximum discharge capacity of 3635 mAh·g^{-1}, which is very close to the theoretical electrochemical hydrogen storage capacity of Si electrode. The a-Si:H thin film deposited by rf-sputtering followed by hydrogenation was also reported to have an electrochemical discharge capacity of 2377 mAh·g^{-1} by the same research team [18].

It can be found that the Si material has a dramatic hydrogen storage capacity, and the a-Si:H electrode has a better electrochemical discharge capacity than the hydrogen-less a-Si electrode. However, the underlying reasons of hydrogenation affecting the electrochemical performance of the a-Si electrode are unknown. The relationship between hydrogen storage capacity and the electrochemical discharge capacity of a-Si:H electrode is also indeterminate. In this work, the a-Si:H thin film was prepared by a two-step process of deposition followed by hydrogenation. By comprehensively comparing the surface morphology, structure, hydrogen content, ionic liquids wettability, and electrochemical performance of the thin films before and after hydrogenation, a preliminary analysis for the mechanism of hydrogenation influence on the structure and electrochemical properties of the a-Si:H thin film electrode was performed.

Experimental

Hydrogen-less a-Si thin films, with the thickness of about 1 μm, were deposited on nickel substrates (diameter 9 mm, purity 99.99%) without substrates heating using conventional rf-magnetron sputtering apparatus. To ensure accurate mass measurements, the mass of film sample was designed to approximately 20 times the sensitivity of the electronic analytical balance (MS105DU, Mettler Toledo). Then, the thickness for films was measured using a surface profiler (MicroXAM-800, KLA-Tencor). In order to increase the binding force between the film and the substrate, the substrate was sandblasted to increase the surface roughness before deposition. To enhance the conductivity of the films, a boron-doped monocrystalline silicon target (75 mm diameter and resistivity less than 0.001 Ω•cm) stuck to the high purity copper back plate was employed to the sputter deposition source. Typical sputter deposition parameters include 0.5 Pa glow discharge pressure, rf (13.56 MHz) power of 300 W, 50 V reverse bias voltage, a target-substrate distance of 75 mm, and pre-sputtered for 5 min to remove the oxides on the silicon target surface. In order to investigate the effect of ex situ hydrogenation on the structure and electrochemical properties of film samples, the as-deposition of a-Si thin films is followed by the hydrogenations conducted in a steel reactor with an inner diameter of 11 mm at 300 ℃, 5 MPa and 500 ℃, 1 MPa, respectively.

To avoid the influence of high energy ion beam generated from focused ion beam (FIB) on the structure of a-Si thin films during the peeling process, the a-Si thin films were deposited on the nickel substrate with a smooth surface first. Then, the a-Si:H powders that fell off naturally from the substrate during hydrogenation were used for transmission electron microscope measurements. For infrared measurements, the a-Si:H thin films on 380-μm-thick high-resistivity crystalline silicon (c-Si) wafers polished optically on both sides were prepared under the same deposition and hydrogenation conditions. The different steps in the preparation of a-S: H thin films are shown in Fig. 1a.

The structure of thin films was determined by Empyrean X-ray diffractometer (XRD) and JEM2010 transmission electron microscope (TEM). The appearance and composition of the sample surface was analyzed by JSM6700F field emission scanning electron microscope (SEM) and AXIS SUPRA X-ray photoelectron spectroscopy (XPS). The relevant bonding configurations of a-Si:H thin films were determined by analyzing infrared transmittance spectra, which were measured with Nicolet IS5 Fourier transform infrared spectrometer (FTIR) in the wavenumber region from 400 to 4000 cm^{-1} with a 4 cm^{-1} resolution.

The electrochemical charge/discharge tests were performed using a half-cell configuration on HYD-B-5 V/500 μA battery program control tester at constant currents. The working electrode was an a-Si:H thin film on Ni substrate and the counter electrode was a sintered $Ni(OH)_2$ disc with the value of positive capacity divided by negative capacity more than 100. The electrolyte was anhydrous ionic liquids (ILs) electrolyte mixed by glacial acetic acid (CH3COOH, > 99.7%, Lanzhou institute of chemical physics) and 1-ethyl-3-methylimidazolium acetate ([EMIM][AC], > 95%, Lanzhou institute of chemical physics). Cyclic voltammetry (CV) measurements were performed using CHI660D electrochemical workstation in a three-electrode Swagelok cell (Fig. 1b). The reference inserted through the top port of the cell was a saturated Ag/AgCl reference electrode, which has a standard potential of + 0.2 V vs. standard hydrogen electrode (SHE) in a 3.4 M KCl solution. To minimize ohmic drop of electrolyte, reference electrode was located near the working electrode. The range of potential

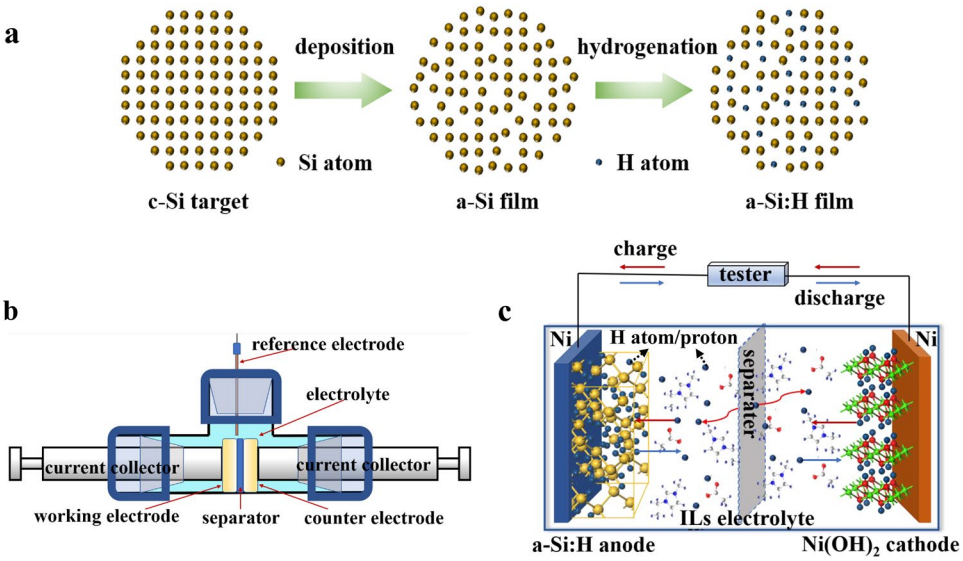

Fig. 1 Illustration of **a** a-Si:H thin film preparation process, **b** structure of electrode, **c** Swagelok cell, and **d** testing/working principle of the battery with a-Si:H electrode and ILs electrolyte

scanning was − 1.7 ~ 0.3 V and the speed of potential scanning was 50 mV/s. The testing and working principle of the battery with a-Si:H thin film electrode and ILs electrolyte is shown in Fig. 1c.

Results and discussion

X-ray diffraction

X-ray diffraction (XRD) studies are performed to investigate the changes in the crystallographic structure of a-Si thin films after ex situ hydrogenation under different conditions. As in Fig. 2, the broad hump centered roughly at 28° is detected in all samples and belongs to an amorphous silicon structure (PDF #27–1420). It's quite clear that the hydrogenations both under 300 ℃, 5 Mpa and 500 ℃, 1 Mpa have not significantly changed the amorphous structure of samples. In addition to this phase, three unusually sharp diffraction peaks, which can be found in the XRD patterns of each sample, are from the metallic nickel substrates. The reason for such a phenomenon is that the film thickness is so small that X-rays scanned at a small angle are transmitted through the thin film to the nickel substrate.

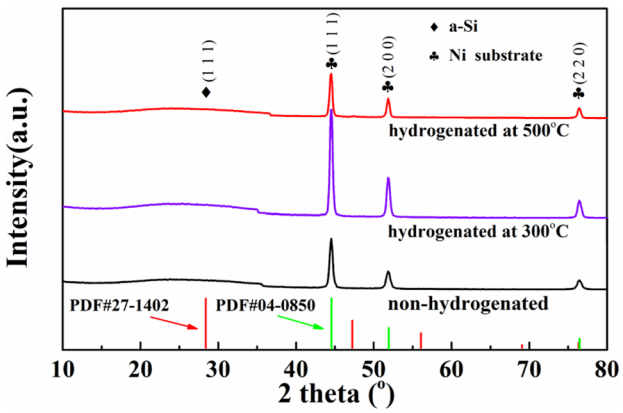

Fig. 2 XRD patterns of a-Si:H thin film hydrogenated at 300 ℃ and 500 ℃

Transmission electron microscope

TEM images of as-deposited a-Si thin film and the a-Si:H thin films hydrogenated at different conditions are shown in Fig. 3a–c, and the electron diffraction patterns are presented in the inset figure. It is not difficult to notice that the obvious amorphization is observed from TEM images of as-deposited a-Si thin film. It is also seen that the electron diffraction patterns in the inset image of Fig. 3a are almost halo, indicating a large extent of amorphization of as-deposited a-Si thin film. Some short-range ordered lattice arrangement can be observed from Fig. 3b–c, and clear rings and few diffraction spots can be found from the inset image. All of this demonstrates that some part of the a-Si:H thin films both hydrogenated at 300 ℃, 5 Mpa and 500 ℃, 1 Mpa transforms into the form of crystallization after hydrogenation. It is evident that the degree and extent of amorphization was markedly reduce in the sample hydrogenated at 500 ℃, 1 MPa compared to the sample hydrogenated at 300 ℃, 5 MPa. This is possibly due to the higher degree of crystallization which is correlated with higher hydrogen pressure of the latter sample. However, the obvious diffraction peaks which belong to the form of crystallization are not observed in the XRD patterns of these samples. These results demonstrated that the amount of crystallization forms in these samples is so little that it's not apparent in the XRD patterns.

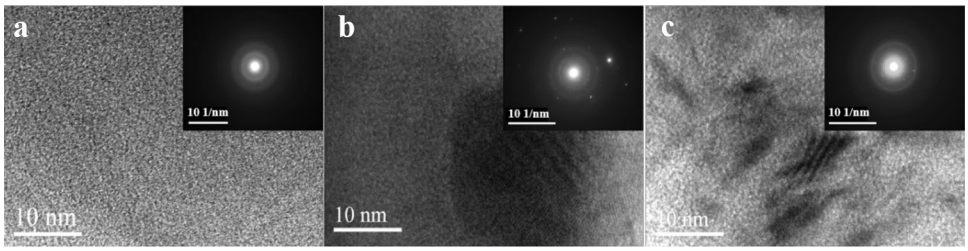

Fig. 3 TEM images and electron diffraction patterns (inset images) of **a** a-Si thin film, a-Si:H thin film hydrogenated at **b** 300 ℃ and **c** 500 ℃

X-ray photoelectron spectroscopy and wettability

In order to investigate the influence of hydrogenation on sample surface, XPS measurements were carried out for samples before and after hydrogenation. As in Fig. 4a, the principal chemical elements used to form samples are silicon and oxygen and the elemental carbon in the spectra is derived from the carbon adsorbed on sample surface, which carbon is probably a result from the sample exposure to air. Figure 4b plots the corresponding high-resolution XPS spectra of samples. After peak fitting, the main products are confirmed to be Si and SiO_2, where the positions are located at 99.5 eV and 103.5 eV, respectively. It can also be found by calculation that the oxide content on the surface of the a-Si:H thin films hydrogenated at 300 ℃ and 500 ℃ increased from initial 7.07 to 23.95% and 44.61%, respectively.

It is obvious that the oxygen content of the sample surface also increased as hydrogenation temperature was increased. The most possible reason is that the sample surfaces are passivated by oxygen atoms adsorbed on the surface of samples and the surface dangling bonds are eliminated, which oxygen atoms probably come from the residual gaseous oxygen in the high-purity compressed gaseous hydrogen.

Furthermore, the wettability of a-Si:H thin films in anhydrous ILs electrolyte was measured using the static contact angle method. As shown in Fig. 5, the average wetting angle between the anhydrous ILs electrolyte and the thin films hydrogenated at 300 ℃ and 500 ℃ is decreased dramatically from the initial degree of 51.3 to 44° and 34.3°, respectively. After hydrogenated at 500 ℃, the wettability of sample in ILs electrolyte changes significantly better than that of the as-deposited a-Si film, which wetting angle decreased by about 33% compared to the latter.

It is possible that the better ILs wettability for the former sample may be associated with the hydrogen-bonded structure and higher content of oxides on its surface [19]. Obviously, the smaller wetting angle is suspected to increase the contact area between the surface of thin film and the ILs electrolyte, which can significantly improve the electrochemical performance of a-Si:H thin film electrode in ILs electrolyte.

Fourier transform infrared spectrometer

In order to obtain the bonding configurations of a-Si:H thin films from the measured transmittance spectra, the sample transmittance was divided by the bare-substrate transmittance and multiplied by 0.54, the absorption-free transmission of c-Si [20, 21]. As shown in Fig. 6, the spectrums of a-Si:H thin films hydrogenated at 300 ℃ and 500 ℃ are dominated by one width strong absorption in the 800 ~ 1000 cm^{-1} region and two evident weak absorption bands, one near 630 cm^{-1} and the second at approximately 2000 cm^{-1}. As

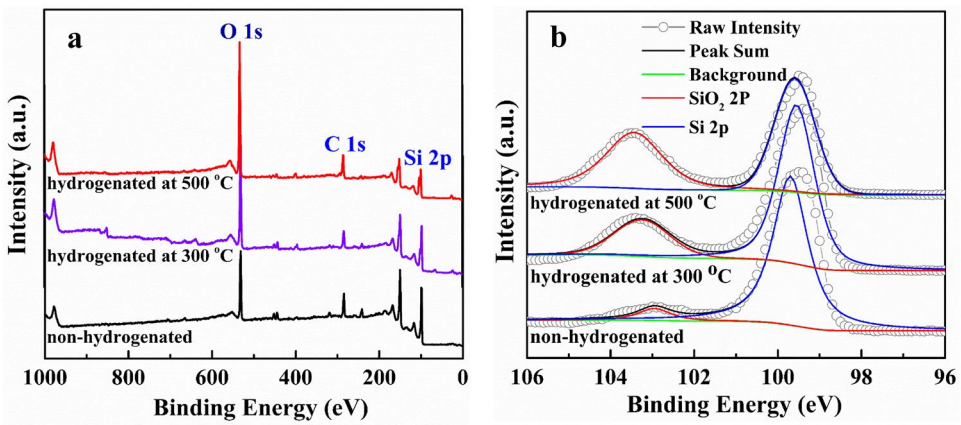

Fig. 4 **a** XPS survey scans and **b** high-resolution XPS spectra with the peak fitting components of a-Si:H thin films

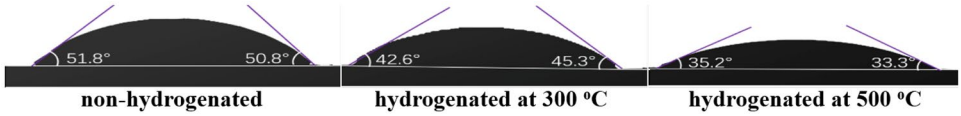

Fig. 5 Wetting angle at the interface between anhydrous ILs electrolyte and a-Si thin film electrode

shown in the partial enlarged spectrogram, the absorption of the latter sample in the 2000–2010 cm^{-1} region consists of a relatively broad and strong component at 2000 cm^{-1} and an additional weaker component at about 2090 cm^{-1}. Of these, the absorption band near 630 cm^{-1} and at approximately 2000 cm^{-1} is assigned to the wagging vibrational mode and stretching mode of Si monohydride (Si–H), respectively. The absorption band in the 800 ~ 1000 cm^{-1} region and at about 2090 cm^{-1} is due to the bending vibrational and stretching modes of Si dihydride ($Si-H_2$) and poly-hydride complexes $(Si-H_2)_n$, respectively.

It is obvious that the absorption bands both at 2000 cm^{-1} and in the bending region due to $Si-H_2$ and $(Si-H_2)_n$ chains for the latter sample are distinctly stronger than that of sample hydrogenated at 300 ℃. Combined with the appearance of new absorption peak near 2090 cm^{-1}, a preliminary qualitative conclusion can be drawn that the sample hydrogenated at 500 ℃ has a relatively higher hydrogen content than the other sample. The significant factor leading to the hydrogen content increases of samples may be that the higher temperature increases the decomposition of hydrogen molecule, the vibrational kinetic energy of hydrogen atoms in the gaseous hydrogen and that of the silicon atoms on the surface of the a-Si:H thin films. That is, as the temperature of hydrogenation increases, the probability of hydrogen atoms being absorbed in the thin films increases.

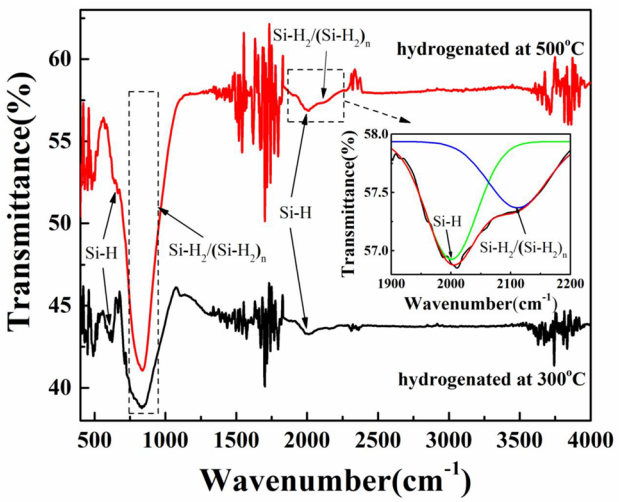

Fig. 6 FTIR spectra of a-Si:H thin films after hydrogenation under different conditions

Electrochemical test

Figure 7 shows the electrochemical charge/discharge curve and the cycling test curve of the a-Si:H thin film electrode before and after hydrogenation. The a-Si:H thin film electrode was charged to 4000 $mAh \cdot g^{-1}$ at the current density of 2000 $mA \cdot g^{-1}$ (0.5C) and discharged at 200 $mA \cdot g^{-1}$ until a cutoff voltage at 0.6 V vs. the $Ni(OH)_2$ counter electrode. As in Fig. 7a, it can be found that the significant improvement on the electrochemical discharge capacity of samples can be realized with the hydrogenation. The discharge capacities of samples hydrogenated at 300 ℃ and 500 ℃ increased from initial 180 to 316 $mAh \cdot g^{-1}$ and 1827 $mAh \cdot g^{-1}$, respectively. Of these, the discharge capacities of sample hydrogenated at 500 ℃ increase over tenfold that of as-deposited a-Si thin film, which reaches almost five times than that of the conventional hydrogen storage alloy used in Ni/MH batteries.

In addition, the discharge potential of a-Si:H electrode hydrogenated at 500 ℃ is lower than others. This may be due to the hydrogenation treatment causing an increase in resistivity near the surface of sample and the higher resistance results in a greater electrode polarization [22]. It was reported that H atoms can break strained Si–O bonds in amorphous silicon dioxide (SiO_2) networks and diffuse in the SiO_2 layer [23, 24]. Maybe the high resistivity of SiO_2 layer on the sample surface influences the electrical transport properties at the interface between the electrolyte and thin film electrode, but it has no considerable effect on the H atoms' diffusion within this interface, which is one of the reasons for the thin film electrode hydrogenated at 500 ℃ to exhibit a high discharge capacity in the case of low discharge potential.

As in Fig. 7b, the discharge capacities of sample hydrogenated at 300 ℃ keeps increasing slowly during the cycling test, but that of sample hydrogenated at 500 ℃ begins to decay rapidly after reaching the maximum discharge capacity in the fifth cycle and which has a relatively higher charge/discharge over-potential than others. This result could be due to the reasons that some oxides appear on the surface and partial crystallization occurs inside the films during hydrogenation, which obstructed effective diffusion range of hydrogen atoms on the surface and inside the films. A number of new irreversible bonds may be formed during the adsorption and desorption process, which leads to a sharp decline in electrochemical capacity.

The cyclic voltammetry curve of a-Si thin film electrode before and after hydrogenation is shown in Fig. 8.

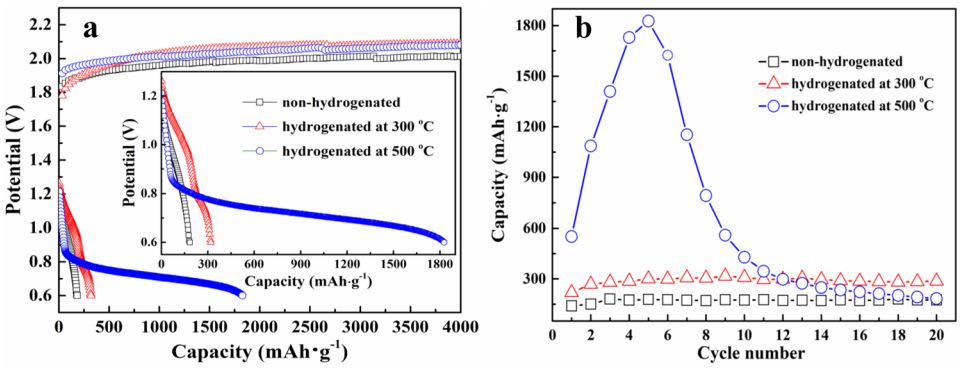

Fig. 7 **a** Electrochemical charge–discharge curve and **b** cycling test of a-Si:H thin film electrode

The obvious anode and cathodic peaks are observed at near − 0.2 V and − 1.0 V vs. reference electrode, which respectively results from oxidation and reduction at the electrode/electrolyte interface. The peak current of the sample after hydrogenation increased sharply and that of the sample hydrogenated at 500 ℃ is the largest, which probably has higher electrochemical activity than others. The reductive peaks on reversal on these cyclic voltammetry curves correspond to the charging process. During this process, a mass of protons in the electrolyte are adsorbed on the surface of a-Si:H thin films after capturing electrons. Under the action of external voltage and concentration gradient, protons of electrolyte diffuse through the electrode/electrolyte interface and occupied on the inner dangling bond of a-Si:H thin film. In contrast, the cathodic peaks for the forward scan correspond to the oxidation reaction of hydrogen. During this process, lots of hydrogen atoms inside the film diffuse toward the interface between electrode and electrolyte and form protons after losing electrons, and then diffuse from the interface to the inside of the electrolyte. The chemical reaction for this reversible process probably occurs as follows [18].

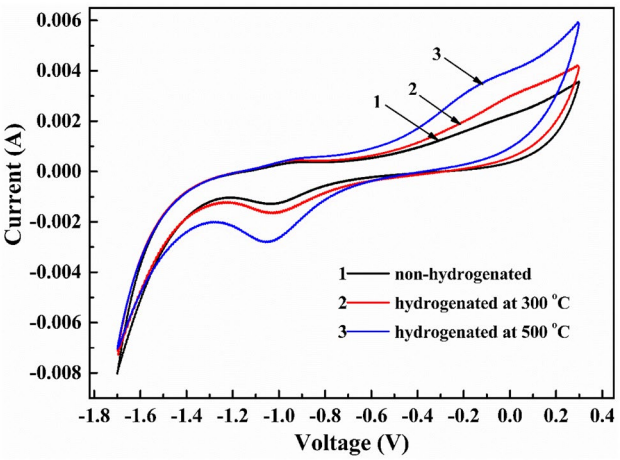

Fig. 8 Cyclic voltammetry curve of a-Si:H thin film electrode

$$\begin{aligned} &\mathrm{Si} + x\mathrm{H}^{+} + xe^{-} \underset{\text{discharge}}{\overset{\text{charge}}{\longleftrightarrow}} \mathrm{SiH}_{\text{x - ad}} \\ &\mathrm{SiH}_{\text{x - ad}} \underset{\text{discharge}}{\overset{\text{charge}}{\longleftrightarrow}} \mathrm{SiH}_{\text{x - ab}} \end{aligned} \quad (1)$$

where SiH_x is silicon hydride and the subscripts "ad" and "ab" denote adsorbed and absorbed, respectively.

In addition, the ratio of peak currents, i_{pa}/i_{pc}, for samples hydrogenated at 500 ℃ is calculated to be approximately 0.83, which is obviously much closer to the Nernstian wave with stable product (the ratio equals 1 [25]) compared to the ratio of 0.63 for as-deposited a-Si thin film. It is demonstrated that the electrochemical reversible performance of the a-Si:H thin film electrode is significantly enhanced by hydrogenation.

The charge–discharge curves of a-Si:H thin film electrode hydrogenated at 500 ℃, 1 MPa for 2 h with different charging current densities are shown in Fig. 9a. The a-Si:H electrode was charged to 4000 mAh·g^{-1} at a rate of 500 mA·g^{-1}, 1000 mA·g^{-1}, 2000 mA·g^{-1}, and 2750 mA·g^{-1}, respectively. It is observed that electrode polarization is caused by the sharp increase of potential difference (PD) with the increase of charging current density. The electrochemical discharge capacity and coulomb efficiency of the a-Si:H thin film electrode are also increased obviously. That result probably comes from the higher potential difference and the greater concentration of hydrogen atoms near the electrode–electrolyte interface, which increases with the increasing charging current density. The high potential difference and the great hydrogen atom concentration can enhance the diffusion rate of hydrogen atoms, which increases the probability of hydrogen atoms diffused through the electrode/electrolyte interface to saturate the defects and dangling bonds inside films. In the process of charging, the diffusion rate of hydrogen atoms in films is lower than in electrolytes due to the lower conductivity of a-Si:H thin film electrode. This provides a potential gradient for hydrogen atoms diffused from electrolyte to the inner of electrode. In short, the

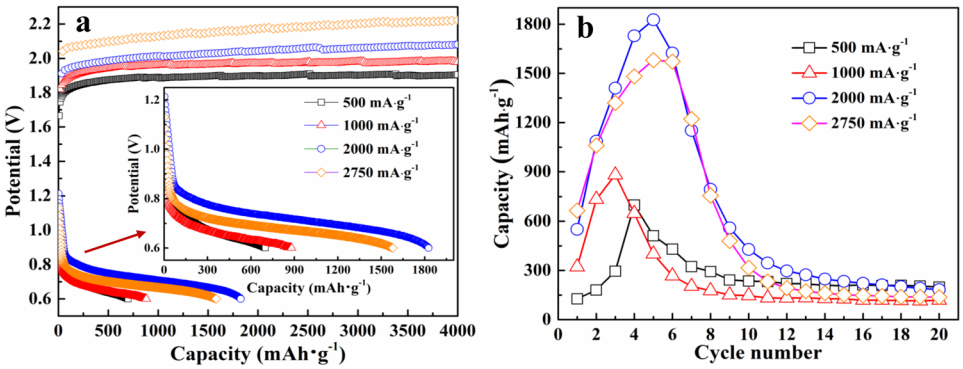

Fig. 9 **a** Electrochemical charge–discharge curve and **b** cycling test of a-Si:H thin film electrode at different charge current densities

increase of electrochemical capacity probably results from the excellent diffused performance of hydrogen atoms with the larger charging current.

As shown in Fig. 9b, both the electrochemical discharge capacity and cycling stability of a-Si:H films electrode modestly increase with the increase of charging current density. However, for the sample charged at a rate of 2000 mA·g^{-1}, although it has a higher electrochemical discharge capacity, cycling stability gets worse and the battery system deteriorates sharply from the 5th cycle. The reason might be the greater charging current exacerbates deteriorating film electrode. The hydrogen concentration near the electrode–electrolyte interface with a larger charging rate is much larger than the numbers of the hydrogen atoms which can be absorbed in films. The extra hydrogen atoms combine with each other to form gaseous hydrogen, which exacerbates the irreversible loss of protons from ILs electrolyte.

To investigate discharging performance, the a-Si:H thin film electrode hydrogenated at 500 ℃ was charged to 4000 mAh·g^{-1} at a rate of 2000 mA·g^{-1} and discharged at the rate of 50 mA·g^{-1}, 200 mA·g^{-1}, 500 mA·g^{-1}, 1000 mA·g^{-1}, and 1500 mA·g^{-1}, respectively. As shown in Fig. 10a, as the discharging current density increases, the discharge capacities of thin film electrodes first increase from 1401 to 1827 mAh·g^{-1} and then decline to 932 mAh·g^{-1}, 310 mAh·g^{-1}, and 169 mAh·g^{-1}, respectively. This result may be due to the exacerbation severity of electrodes which increase sharply with the increasing discharged current. Figure 10b shows the electrochemical discharge capacity and Coulomb efficiency as a function of charge capacity for a-Si:H thin film electrode. During the test, the a-Si:H electrode was charged to 1000 mAh·g^{-1}, 2000 mAh·g^{-1}, 3000 mAh·g^{-1}, and 4000 mAh·g^{-1} at the same charging rate of 2000 mA·g^{-1} and discharged at the same current density of 200 mA·g^{-1}. It can be found that the electrochemical discharge capacity of samples increases with increasing the charged capacity, but the samples have poor Coulomb efficiency, which showed similar values of around 46 to 57%. This might be attributed to some defects and unstable structure in the thin film electrodes hindering the diffusion of H atom in the interior of the thin film electrodes, which affected the reversibility of electrode structure during the charge/discharge process.

Scanning electron microscopy

SEM micrographs were taken for a-Si thin films before hydrogenation. As shown in Fig. 11 a and b, as-deposited a-Si thin film exhibits a rough and lumpy surface and the average film thickness was about 965.3 nm, which is mostly consistent with the results obtained using surface profiler. As shown in Fig. 11 c and d, the surface of a-Si:H thin films after hydrogenation has no significant change except some fine particles of powder produced, which probably result from the expansion/contraction of samples

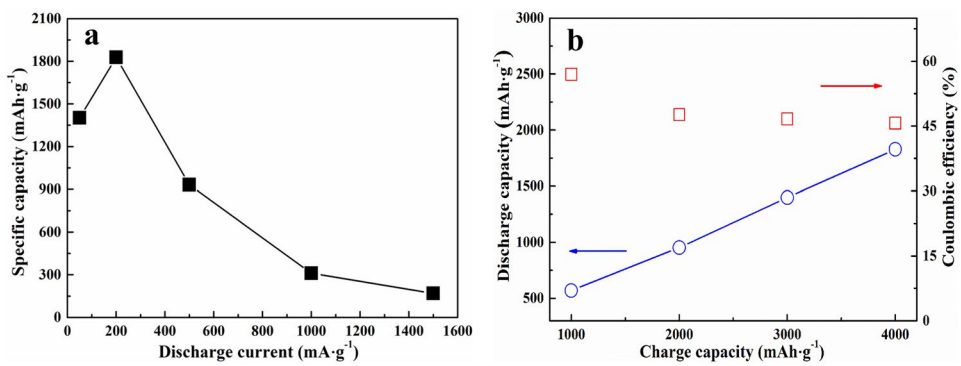

Fig. 10 **a** Rate capability for a-Si:H thin film electrode at different discharging current densities and **b** discharge capacity and Coulomb efficiency as a function of charge capacity for a-Si:H thin film electrode.

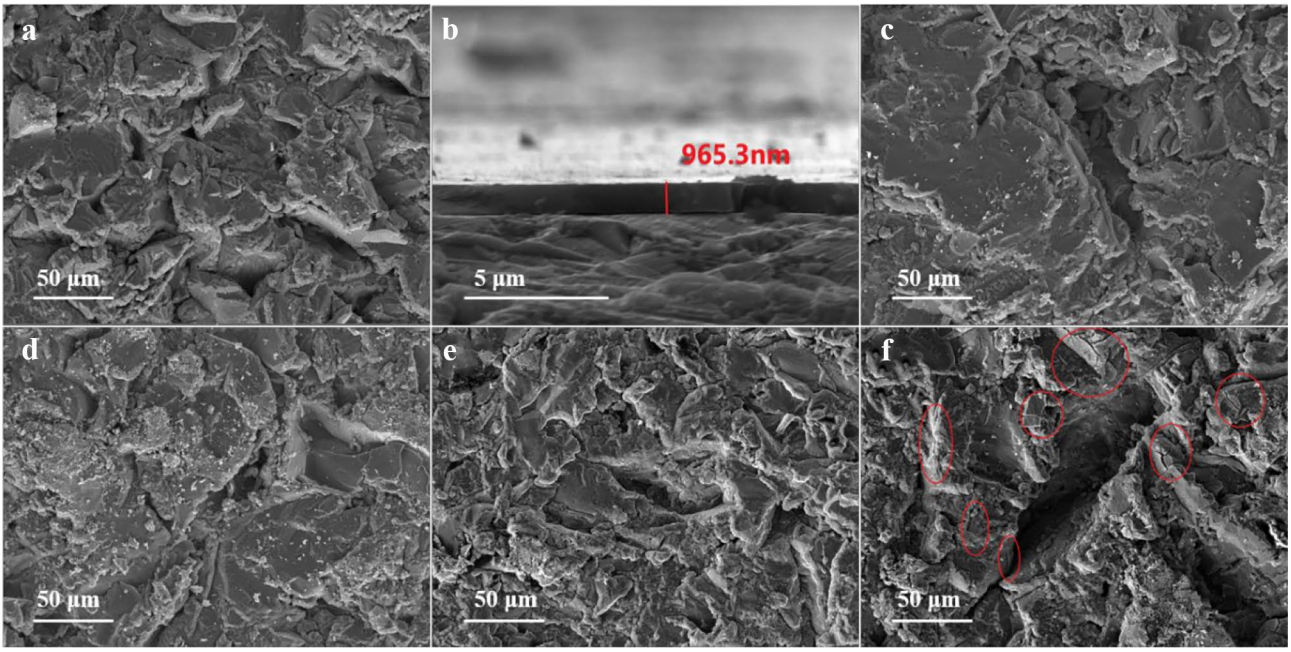

Fig. 11 SEM images of **a** the surface and **b** the cross-section of as-deposited a-Si thin film, and surface of films hydrogenated at **c** 300 ℃ and **d** 500 ℃, and surface of film hydrogenated at 500 ℃ after 25 cycles at a charge rate of **e** 200 $mA{\cdot}g^{-1}$ and **f** 2000 $mA{\cdot}g^{-1}$

during hydrogenation/dehydrogenation. The powdering of film surface is may be attributed to hydrogen damage during the hydrogenation treatment as reported in the literature [26]. Moreover, in addition to bonding with the dangling bonds on the a-Si surface, the hydrogen atoms can be diffused into the a-Si bulk when enough hydrogen covers the surface [27, 28]. The surface of sample hydrogenated at 500 ℃ has much more particles than hydrogenated at 300 ℃, which indicated that more amounts of hydrogen react with a-Si film surface and more hydrogen diffused into the a-Si bulk for 500 ℃ hydrogenation. Therefore, we speculate that more hydrogen in the a-Si:H film hydrogenated at 500 ℃ may be one of the reasons for its higher electrochemical capacity than others.

To find out the causes of electrochemical capacity degradation for a-Si:H thin film electrode, the SEM surface images of sample hydrogenated at 500 ℃ after 25 cycles are shown in Fig. 11 e and f, which was charged to 4000 $mAh{\cdot}g^{-1}$ at a rate of 200 $mA{\cdot}g^{-1}$ and 2000 $mA{\cdot}g^{-1}$, respectively. The very serious cracking on the surface of sample at the charging rate of 2000 $mA{\cdot}g^{-1}$ is observed in contrast to the no obvious changed surface microstructure of sample charged at the rate of 200 $mA{\cdot}g^{-1}$. This result could be due to the small current which cannot destroy the interfacial bonding between the film and the substrate, and the large-scale cracking phenomenon appears to result from the dramatic expansion/contraction of samples during adsorption/desorption. The contact resistance increases due to the cracking and the poor physical contact between the a-Si:H thin film and the nickel substrate, which makes the electrode polarization trend more serious.

For this new type of Ni-MH battery, it could be determined that the proton hops through the hydrogen-bond network in ILs electrolyte according to Grotthuss mechanism [29]. However, two possible models for hydrogen diffusion in a-Si:H thin film are reported. One assumes that the hopping of hydrogen atoms appears between dangling bond sites and the diffusion properties probably depend on the hydrogen concentrations and dangling bonds in the film [30]. In the alternative model, the hydrogen hops directly from one Si–H bond to another [31, 32]. As far as we are concerned, the two models appear to correspond to different experimental environments and initial conditions for hydrogen diffusion. For instance, during the hydrogenation and electrochemical charging processes, the hydrogen atoms located on the edge of the Si–H bonds network, under the pressure of high potential energy difference, have to hunt down a smaller barrier bonds to occupy or hopping for diffusion; thus, the hanging bonds and few low-bonding energy Si–Si bonds become the best candidates. That may be one of the suspected causes of the better electrochemical performance can be activated by a larger amount of charged current density. In contrast, during the thermal desorption and electrochemical discharging processes, the exchange of diffusion hydrogen atoms between Si–H bond sites can occur with lower activation barriers than needed for excitation of a single hydrogen out of an Si–H bond [33]; thus, the smaller discharge current can provide the energy for hydrogen atoms

diffusion easily inside the a-Si:H film. Compared to hopping from one dangling bond site to another, the exchange of hydrogen atoms between Si–H bonds appears to need less activation energy from outside. The higher hydrogen concentration probably provides more Si–H bonds for the hopping of hydrogen atoms, which increases the diffusion rate of hydrogen atoms and the active sites for reversible hydrogen absorption and desorption in the a-Si:H thin film.

In addition, although the a-Si:H thin film electrode prepared in this work has a maximum electrochemical discharge capacity of 1827 $mAh{\cdot}g^{-1}$, the cycle performance and Coulomb efficiency of which are much worse than conventional alloy electrodes. We propose several significant factors leading to the capacity degradation of a-Si:H thin film electrode as follows. (1) The a-Si:H thin film electrode usually has a high resistivity (about 107 ~ 109 Ω•cm), which has a relatively high electrode polarization during the electrochemical test. (2) Partial crystallization and oxidation are found on the surface and inner of a-Si:H thin film after hydrogenation, which decreases the active sites of hydrogen atoms absorbed on the surface and diffused inside films. (3) The large-scale cracking of a-Si:H thin film electrode results from the expansion/contraction of samples during hydrogenation/dehydrogenation. (4) The lower hydrogen content of the prepared samples leads to the less active sites for hydrogen diffusion and absorption, which decreases the electrochemical discharge capacity of a-Si:H thin film electrode. (5) Some protons in anhydrous ILs electrolyte compound produce gaseous hydrogen during the electrochemical charged process, thus reducing the number of protons that can be used to participate in adsorption/absorption.

Conclusions

The a-Si:H thin films, with the thickness of about 1 μm, were prepared by a tow-step process of rf-sputtering followed hydrogenation and the effect of hydrogenation on the structure and electrochemical properties of a-Si:H thin film electrode was studied systematically. Then, the preliminary relationships between hydrogen content and electrochemical performance and the significant factors leading to the capacity degradation for a-Si:H thin film electrode were analyzed. The result shows that the maximum electrochemical discharge capacities of a-Si:H thin film electrodes hydrogenated at 500 ℃ increased from initial 180 to 1827 $mAh{\cdot}g^{-1}$, which is over tenfold that of as-deposited a-Si thin film. The higher hydrogen concentration of a-Si:H thin film resulted from hydrogenation appears to provide more Si–H bonds for the hopping of diffusion hydrogen atoms and more active sites for reversible hydrogen absorption and desorption. However, the cycle performance and Coulomb efficiency of a-Si:H thin film electrode is worse, which probably due to the deterioration of electrolyte, and the high resistivity, partial crystallization and oxidation, large-scale cracking, and lower hydrogen content of samples.

Funding This work is financially supported by national natural science foundation of china (22065020).

References

1. Davis SJ, Caldeira K, Matthews HD (2010) Future CO_2 emissions and climate change from existing energy infrastructure. Science 329:1330–1333
2. Chalk SG, Miller JF (2006) Key challenges and recent progress in batteries, fuel cells, and hydrogen storage for clean energy systems. J Power Sources 159:73–80
3. Rusman NAA, Dahari M (2016) A review on the current progress of metal hydrides material for solid-state hydrogen storage applications. Int J Hydrogen Energy 41:12108–12126
4. Tliha M, Mathlouthi H, Lamloumi J, Percheron-Guégan A (2011) Electrochemical study of intermetallic metal hydride as an anode material of Ni-MH batteries. J Solid state Electrochem 15:1963–1970
5. George L, Saxena SK (2010) Structural stability of metal hydrides, alanates and borohydrides of alkali and alkali- earth elements: a review. Int J Hydrogen Energy 35:5454–5470
6. Zhang W, Han S, Hao J, Li Y, Bai T, Zhang J (2009) Study on kinetics and electrochemical properties of low-Co AB_5-type alloys for high-power Ni/MH battery. Electrochim Acta 54:1383–1387
7. Ruiz FC, Castro EB, Peretti HA, Visintin A (2010) Study of the different Zr_xNi_y phases of Zr-based AB_2 materials. Int J Hydrogen Energy 35:9879–9887
8. Chi Y, Weng WX, Wang ZM, Li C (2008) Self-discharge behavior of $LaNi_5$-based hydrogen storage electrodes in different electrolytes. J Solid state Electrochem 12:935–940
9. Stuckelberger M, Biron R, Wyrsch N, Haug F-J, Ballif C (2017) Review: Progress in solar cells from hydrogenated amorphous silicon. Renew Sustain Energy Rev 76:1497–1523
10. Yamaguchi K, Domi Y, Usui H, Shimizu M, Matsumoto K, Nokami T, Itoh T, Sakaguchi H (2017) Influence of the structure of the anion in an ionic liquid electrolyte on the electrochemical performance of a silicon negative electrode for a lithium-ion battery. J Power Sources 338:103–107
11. Trill JH, Tao C, Winter M, Passerini S, Echert H (2011) NMR investigations on the lithiation and delithiation of nanosilicon-based anodes for Li-ion batteries. J Solid state Electrochem 15:349–356
12. Kale P, Gangal AC, Edla R, Sharma P (2012) Investigation of hydrogen storage behavior of silicon nanoparticles. Int J Hydrogen Energy 37:3741–3747
13. Lan JH, Cheng DJ, Cao DP, Wang WC (2008) Silicon nanotube as a promising candidate for hydrogen storage: from the first principle calculations to grand canonical Monte Carlo simulations. J Phys Chem C 112:5598–5604
14. Zhang D, Ma C, Liu C (2007) Potential high-capacity hydrogen storage medium: hydrogenated silicon fullerenes. The Journal of Physical Chemistry C 111:17099–17103
15. Song B, Zhang C, He P (2015) $Si_{20}H_{20}$ cluster modified by small organic molecules and lithium atoms for high-capacity hydrogen storage. Int J Hydrogen Energy 40:8093–8105
16. Merazga S, Cheriet A, M'hammedi K, Mefoued A, Gabouze N (2019) Investigation of porous silicon thin films for electrochemical hydrogen storage. Int J Hydrogen Energy 44:9994–10002

17. Honarpazhouh Y, Astaraei FR, Naderi HR, Tavakoli O (2016) Electrochemical hydrogen storage in Pd-coated porous silicon/graphene oxide. Int J Hydrogen Energy 41:12175–12182
18. Meng T, Young K, Beglau D, Yan S, Zeng P, Cheng MM-C (2016) Hydrogenated amorphous silicon thin film anode for proton conducting batteries. J Power Sources 302:31–38
19. Grundner M, Jacob H (1986) Investigations on hydrophilic and hydrophobic silicon (100) wafer surfaces by X-ray photoelectron and high-resolution electron energy loss-spectroscopy. Appl Phys A 39:73–82
20. Lucovsky G, Nemanich RJ, Knights JC (1979) Structural interpretation of the vibrational spectra of a-Si: H alloys. Phys Rev B 19:2064–2073
21. Maley N (1992) Critical investigation of the infrared-transmission-data analysis of hydrogenated amorphous silicon alloys. Phys Rev B Condens Matter 46:2078–2085
22. Pankove JI, Carlson DE, Berkeyheiser JE, Wance RO (1983) Neutralization of shallow acceptor levels in silicon by atomic hydrogen. Phys Rev Lett 51:2224–2225
23. El-Sayed AM, Watkins MB, Grasser T, Afanas'ev VV, Shluger AL (2015) Hydrogen-induced rupture of strained Si-O bonds in amorphous silicon dioxide. Phys Rev Lett 114:115503
24. Sheikholeslam SA, Manzano H, Gresu C, Ivanov A (2016) Reduced hydrogen diffusion in strained amorphous SiO2: undestanding ageing in MOSFET devices. Journal of Materials Chemistry C 4:8104–8110
25. Bard AJ, Faulkner LR (2001) Electrochemical Methods: Fundamentals and Applications. John Wiley & Sons Inc, New York
26. Tsai JW, Huang CY, Tai YH, Cheng HC, Su FC, Luo FC, Tuan HC (1997) Reducing threchold voltage shifts in amorphous silicon thin film transistors by hydrogenating the gate niride prior to amorphous silicon deposition. Spplied Physics Letters 71:1237–1239
27. Mortensen K, Chen DM, Bedrossian PJ, Golovchenko JA, Besenbacher FB (1991) Two reaction channels directly observed for atomic hydrogen on the Si(111)-7×7 surface. Phys Rev B 43:1816–1819
28. Teresi CS, Gerberich WW (2018) Silicon activation volumes for fracture as affected by hydrogen. Scripta Mater 144:56–59
29. Yasuda T, Watanabe M (2013) Protic ionic liquids: fuel cell applications. MRS Bull 38:560–566
30. Carlson DE, Magee CW (1978) A SIMS analysis of deuterium diffusion in hydrogenated amorphous silicon. Appl Phys Lett 33:81–83
31. Jackson WB, Tsai CC (1992) Hydrogen transport in amorphous silicon. Phys Rev B Condens Matter 45:6564–6580
32. Street RA, Tsai CC, Kakalios J, Jackson WB (1987) Hydrogen diffusion in amorphous silicon. Philosophical Magazine B 56:305–320
33. Street RA (2011) Hydrogen Diffusion and Thermal Equilibrium of Electronic States in a-Si:H. MRS Online Proc Libr. https://doi.org/10.1557/proc-95-13